Int. J. Solids Structures Vol. 26, No. 5/6, pp. 631–642, 1990
Printed in Great Britain.

0020–7683/90 $3.00 + .00

EFFECTS OF INTERFACE DEBONDING ON THE TOUGHNESS OF DUCTILE–PARTICLE REINFORCED CERAMICS

GANG BAO† and CHUNG-YUEN HUI
Department of Theoretical and Applied Mechanics, Cornell University, Ithaca, NY 14853, U.S.A.

(*Received* 13 *December* 1988; *in revised form* 28 *May* 1989)

Abstract—A debonding–stretching model is proposed in this work to analyse the effects of interfacial debonding on the ductile particle toughening of ceramics. Perfect bonding imposes lateral constraints on the particles thus prohibiting the full utilization of the particle's inherent ductility. In contrast, partial debonding increases the plastic stretching which leads to a larger crack opening displacement in the bridging zone. The theoretical prediction of the fracture toughness based on the debonding–stretching model is closer to that measured by experiments. A continuous model based on the micro-mechanical analysis of the plastically stretched particles is used to calculate the deformation field in the bridging zone for a Mode I plane strain crack loaded under small scale bridging condition. The length of the bridging zone is determined numerically as a function of the applied stress intensity factor and relevant material parameters.

1. INTRODUCTION

Extensive theoretical and experimental studies have been devoted to enhance the fracture toughness of brittle materials. Apart from transformation toughening (McMeeking and Evans, 1982; Budiansky *et al.*, 1983), ceramic fiber toughening (Budiansky *et al.*, 1986) and microcrack shielding (Hutchinson, 1987), ductile particle toughening is another mechanism to achieve additional toughness. By dispersing partly oxidized aluminium particles in a glass matrix, a 60-fold increase in the toughness has been found (Krstic *et al.*, 1981). Recent investigations also reveal a significant metal dispersion toughening in Al_2O_3/Al and WC/Co systems (Sigl *et al.*, 1988). It is believed that the main contribution to composite toughness comes from ligament formation in the matrix and ligament failure behind the advancing crack front.

Theoretical analysis of ductile–particle toughening has been conducted previously based on the crack-bridging model. This model was first introduced by Krstic (1983) assuming that once the crack has reached the particle-matrix interface, it will be locally blunted and forced to circumvent the particle, thus bridging the crack along its length. Budiansky *et al.* (1988) modeled the bridging process by treating the ductile particles as a continuous distribution of springs lying along the crack face. A slip line solution has been employed to estimate the energy release rate due to crack extension (Evans and McMeeking, 1986). Sigl *et al.* (1988) analysed the plastic stretching of a particle both numerically and analytically. Their theoretical prediction is substantially less than the measured toughness which Sigl *et al.* (1988) attributed to residual stress effects. In this paper, we offer another possible mechanism which could explain these discrepancies.

To utilize the ductility of the particles in the toughening process, it is necessary to have a satisfactory bonding between the matrix and the particles. However, partial debonding of the matrix-particle interface can occur due to stress concentration near the crack tip. Debonding relaxes the lateral constraint which could further increase the crack opening displacement in the bridging zone, thus enhancing the toughness of the composite. Indeed, most previous estimates of toughening have been based on the assumption of perfect bonding, although the effect of debonding on the toughening of particle reinforced ceramics has been described qualitatively (Krstic, 1983).

† Now at the Materials Department, University of California, Santa Barbara, CA 93106, U.S.A.

In Section 2, we propose a simple model to obtain an analytical approximation of the plastic stretching u of the ductile particles in terms of local tensile stress σ acting on the crack faces. The method used in our analysis is similar to that employed by Sigl *et al.* (1988), but the effects of debonding have been taken into account. The σ–u relation based on this debonding–stretching model leads to a much higher theoretical estimate of fracture toughness in comparison with that estimated by perfect bonding model.

In Section 3, the σ–u relation resulting from the micro-mechanical analysis in Section 2 is linearized and used as a softening constitutive model to determine the stress field in bridging zone. The length of the bridging zone as a function of the applied load for a plane strain Mode I crack loaded under small scale bridging conditions is obtained by solving the resulting integral equation. The validity of our model is discussed in Section 4.

2. DEBONDING–STRETCHING ANALYSIS

There are several possibilities that crack extension can take place in particle reinforced ceramics: (1) the crack may avoid the particles and propagate only in the matrix; (2) the stress concentration could cause plastic deformation of the particles as well as debonding of the interfaces. In extreme cases, the crack can circumvent the particles via complete debonding. In other cases, partial or no debonding occur and the plastically stretched particles form a bridging zone and crack extension occurs by failure of the stretched particles, as shown in Fig. 1. Since the ductile particles have elastic stiffness less than that of the matrix, the crack is always attracted to particles (Tirosh and Tetelman, 1976).

Figure 2a shows the geometry used by Sigl *et al.* (1988) in their analysis of plastic stretching of the ductile particle in a ceramic matrix. Since no debonding is allowed in their model, the points a and a' shared the same location. This configuration has considerably more lateral constraint than the configuration shown in Fig. 2b in which the debonded interface is denoted by the arc aa'. In the following, we shall assume that the length of the debonded zone aa' is such that the neck geometry shown in Fig. 2b can be realized. Also, we shall assume that the ductile particle is incompressible which implies that $V_1 = V_2$, as shown schematically in Fig. 2b. Specifically, V_1 is the volume to be removed to form the neck geometry and V_2 is the volume added to the neck. Using this assumption, the relation between the crack opening displacement u and the geometry of the neck is found to be (Appendix)

$$u/a_0 = (R/a_0)^2(\pi - 4R/3a_0) \tag{1}$$

where R is the radius of the neck and a_0 is the particle size. Our neck geometry implies that failure of the ductile particle occurs when $R = a_0$. The critical crack opening displacement u^* is obtained by setting $R = a_0$ in eqn (1), i.e.

$$u^* = (\pi - 4/3)a_0 = 1.808a_0 \tag{2}$$

which is about 2.3 times larger than that predicted by the perfect bonding model (Sigl *et al.*, 1988). The enhanced toughness ΔG_p is

$$\Delta G_p = f\int_0^{u^*} \sigma_p(u)\,\mathrm{d}u \tag{3}$$

where f is the area fraction of the ductile particles intercepted by the crack and $\sigma_p(u)$ is the effective restraining normal stress acting on the crack faces due to a particle for a given crack opening displacement u. Following Sigl *et al.* (1988), $\sigma_p(u)$ can be estimated by treating the particle as cylindrically necked bar. The mean axial stress σ_z in the necked region is given by Bridgeman to be:

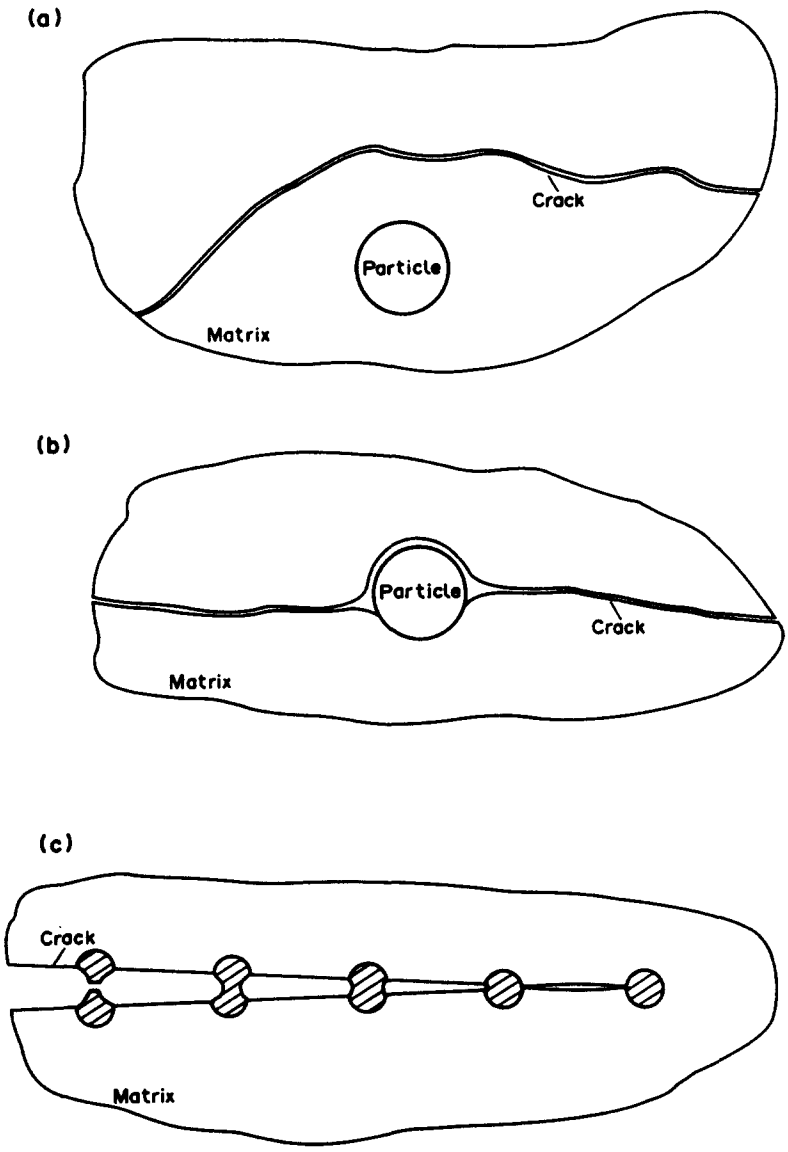

Fig. 1. Schematic illustration of different ways of crack extension in particle-reinforced ceramics. (a) Crack avoids particles. (b) Crack extend by debonding. (c) Crack bridging.

$$\sigma_z = \sigma_f(1+2R/a)\ln(1+a/2R) \tag{4}$$

where a is the neck radius and σ_f is the uniaxial flow stress of the ductile particle. The particle is assumed to behave as a power law hardening material so the σ_f is related to the tensile strain ε by

$$\sigma_f/\sigma_0 = (\varepsilon/\varepsilon_0)^n \tag{5}$$

where σ_0 and ε_0 are the initial yielding stress and strain respectively and n is the hardening coefficient. The restraining normal stress σ_p can now be estimated by

$$\sigma_p = \sigma_z(a/a_0)^2. \tag{6}$$

Equations (4–6) together with

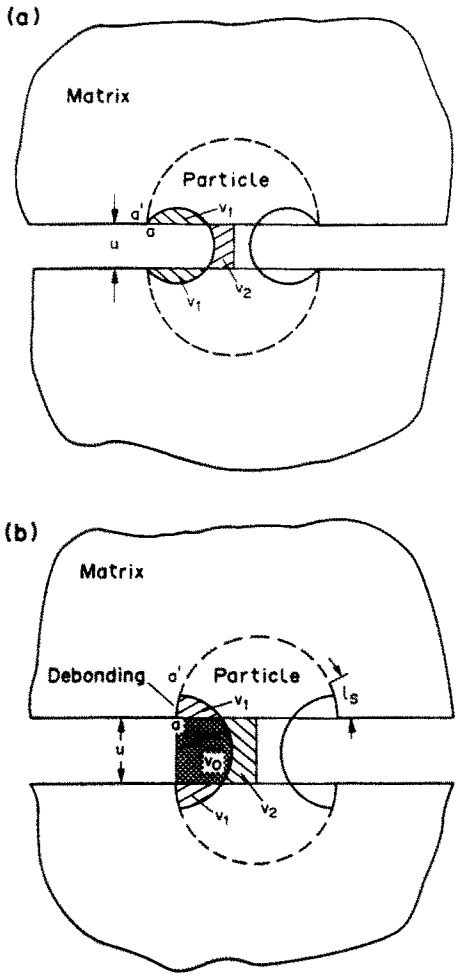

Fig. 2. A schematic diagram of the neck geometry used to estimate the stress on the ductile particle. (a) Perfect bonding model. (b) Debonding–stretching model.

$$\varepsilon = 2 \ln (a_0/a) \tag{7}$$

gives $\sigma_p(u)$ as a function of R, a and a_0, i.e.

$$\sigma_p = 2^n \sigma_0 (\varepsilon_0)^{-n} (1+2R/a) \ln (1+a/2R) [\ln (a_0/a)]^n (a/a_0)^2. \tag{8}$$

The assumed neck geometry implies that $a = a_0 - R$. Consequently, the function $\sigma_p(u)$ can be expressed in terms of a pair of parametric equations, i.e.

$$u/a_0 = x^2(\pi - 4x/3) \tag{9}$$

$$\sigma_p/\sigma_0 = 2^n (1-x^2) \ln [(1+1/x)/2] [-\ln (1-x)]^n / (\varepsilon_0)^n \tag{10}$$

where

$$x = R/a_0. \tag{11}$$

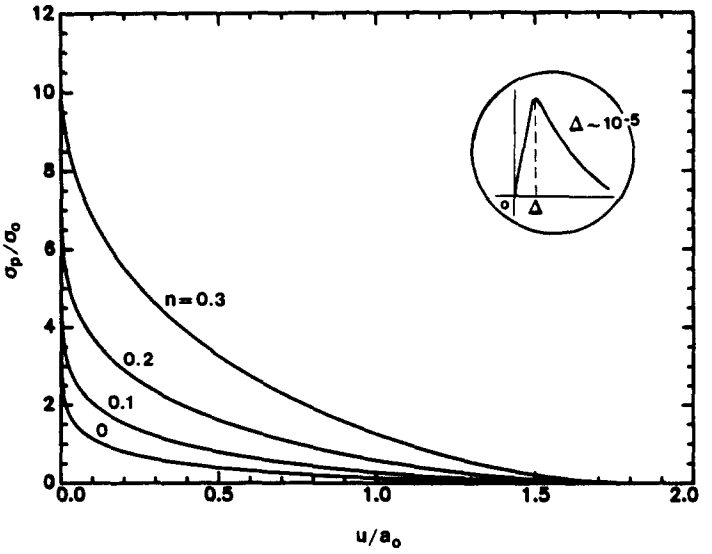

Fig. 3. Plot of normalized stresses vs nondimensional crack opening.

A plot of σ_p/σ_0 vs $\mu = u/a_0$ is given in Fig. 3. Note that for $\mu > \Delta$, the slope of the σ_p/σ_0 vs μ curve is negative. A continuous model of the bridging zone can be obtained by treating σ_p as the normal traction on the bridging zone and $u/2$ as the opening displacement. The material in the bridging zone is said to exhibit softening behavior for $\mu > \Delta$ since the slope of the $\sigma_p(u)$ curve in this region is negative.

The change in toughness defined in eqn (3) is evaluated using eqns (9–11), i.e.

$$\Delta G_p/f\sigma_0 a_0 = 2\pi(\varepsilon_0)^{-n}2^n \int_0^1 x(1-2x/\pi)(1-x^2)\ln[(1+1/x)/2][-\ln(1-x)]^n \, dx. \quad (12)$$

Equation (12) is plotted in Fig. 4 as a function of n with $\varepsilon_0 = 10^{-3}$ and compared with

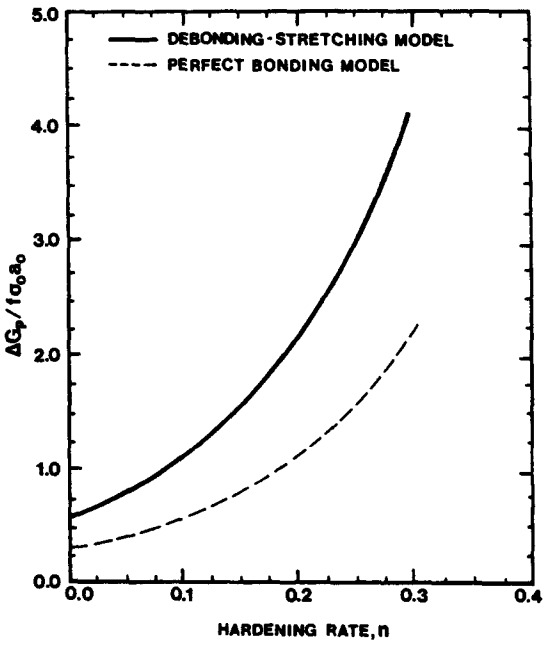

Fig. 4. Effect of debonding on fracture toughness.

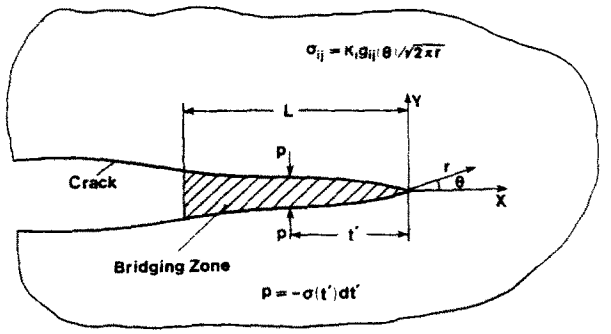

Fig. 5. A schematic diagram of the geometry of the bridging zone.

the perfect bonding result given by Sigl *et al.* (1988). This comparison shows that, for the neck geometry shown in Fig. 2b, the presence of debonding increases the fracture toughness by about 80%.

3. STRESS FIELD IN BRIDGING ZONE

The distribution of tensile stress σ and the crack opening displacement u in the bridging zone can be evaluated by treating the stretched particles as continuously distributed springs with stress-displacement relation $\sigma(u)$, where σ is identified with the smear-out particle stress $f\sigma_p$ defined in Section 2. It is assumed that the bridging zone length is small compared with typical specimen dimensions, e.g. the crack length, so that the crack can be modeled as semi-infinite, as shown in Fig. 5. A Cartesian coordinate system (X, Y, Z) is used with the Z-axis lying along the crack front together with a polar coordinate system (r, θ). Under small scale yielding condition (Rice, 1968), the stress distribution far from the crack tip approaches

$$\sigma_{ij} \sim K_I g_{ij}(\theta)/(2\pi r)^{1/2} \quad \text{as } r \to \infty. \tag{13}$$

Equation (13) is the linear elastic crack tip stress field for the case of Mode I loading. To further simplify the analysis, we approximate the σ–u relation obtained using eqns (9–11) as a straight line. The slope and the intercept of the straight line on the u axis is determined by the conditions:

$$\sigma_c u_c/2 = \int_0^{u^*} \sigma \, du \tag{14}$$

and

$$\sigma_c/u_c = \sigma^*/u^* \tag{15}$$

as shown in Fig. 6. The condition (14) implies that the areas of the $\sigma(u)$ curves are equal so that the resulting G_{IC} are the same. The reason for using eqn (15) will be explained later. The displacement in the bridging zone, $v(X)$, $(v = u/2)$ is related to $\sigma(X)$ by

$$v = u_c(1 - \sigma/\sigma_c)/2. \tag{16}$$

The slope of the straight line (16) is negative indicating that the plastically stretched material in the bridging zone exhibiting softening behavior. On the other hand, $v(X)$ is given by

$$v(X) = v_\infty(X) + v_\sigma(X) \tag{17}$$

where

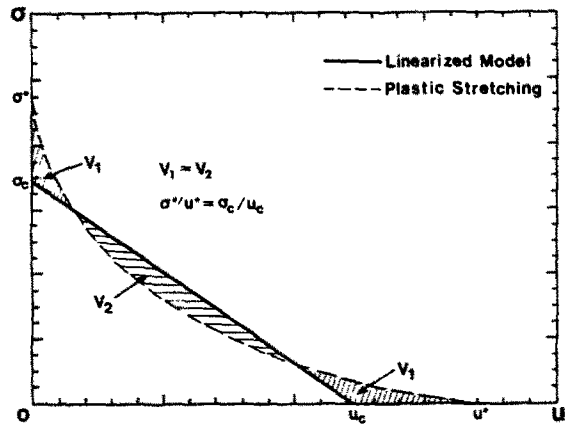

Fig. 6. Comparison of the approximate linear plastic stretching model with the σ–u relation given by eqns (9)–(11).

$$v_\infty(X) = 4K_I(1-\nu^2)|X|^{1/2}/E(2\pi)^{1/2} \tag{18}$$

is the crack opening displacement of a traction free crack due to the stress field eqn (13) applied far from the crack tip. v_σ is the additional crack opening displacement due to $\sigma(X)$ acting on the crack faces and is given by (Tada *et al.*, 1974)

$$v_\sigma = -2(1-\nu^2)/E\pi \int_{-L}^{0} \sigma(t') \ln|(|X|^{1/2}+|t'|^{1/2})/(|X|^{1/2}-|t'|^{1/2})| \, dt' \tag{19}$$

where t' is the local coordinate in the bridging zone as shown in Fig. 5.

With the change of variables $x = -X$, $t = -t'$, eqns (16–19) lead to the following integral equation for $\sigma(x)$

$$u_c(1-\sigma/\sigma_c)/2 = 4K_I(1-\nu^2)x^{1/2}/E(2\pi)^{1/2} - 2(1-\nu^2)/E\pi \int_0^L \sigma(t) \ln|(x^{1/2}+t^{1/2})/(x^{1/2}-t^{1/2})| \, dt. \tag{20}$$

The crack tip is now at $x = L$ and the tip of the bridging zone is at $x = 0$. Using the normalized variables

$$\phi = \sigma/\sigma_c, \quad \xi = x/L, \quad \eta = t/L. \tag{21}$$

Equation (20) becomes

$$1-\phi(\xi) = 2(\lambda\alpha)^{1/2}\xi^{1/2} - \alpha \int_0^1 \phi(\eta) \ln|(\xi^{1/2}+\eta^{1/2})/(\xi^{1/2}-\eta^{1/2})| \, d\eta \tag{22}$$

where the dimensionless parameter

$$\alpha = 4\sigma_c(1-\nu^2)L/\pi E u_c \tag{23}$$

is the normalized zone length and the dimensionless parameter

$$\lambda = 2K_I(1-\nu^2)/E\sigma_c u_c \tag{24}$$

is the ratio of the available energy release rate due to the applied load and the fracture

toughness ΔG_p of the material in the bridging zone. The choice of using eqns (14–15) for the straight line fit of the σ–u relation is justified by the fact that λ and α are completely determined by $\sigma_c u_c$ and $\sigma_c u_c$.

The overall stress intensity factor at the tip of the bridging zone ($\xi = 0$), K_{tip}, is

$$K_{tip} = K_I + K_\sigma \tag{25}$$

where

$$K_\sigma = -L^{1/2}(2/\pi)^{1/2}\sigma_c \int_0^1 \phi(\eta)/(\eta)^{1/2}\,d\eta \tag{26}$$

is the stress intensity factor due to the restraining traction σ acting on the crack faces (Tada *et al.*, 1974). Crack propagation or fracture occurs when σ reaches zero at the crack tip (i.e. $v = u_c/2$ in eqn (16)) and K_{tip} reaches the critical stress intensity of matrix, K_m at the tip of the bridging zone ($\xi = 0$). In general, both these two conditions must be satisfied for crack growth. However, for ductile–particle reinforced ceramics, K_m is rather small compared with the stress intensity factor due to the ductile–particle shielding. Therefore, in this paper, we neglect the effect of K_m, namely, K_m is set to zero. Note that $K_{tip} = 0$ implies that the stress σ at the tip of the bridging zone is bounded. Using eqn (26), the condition $K_{tip} = 0$ is

$$K_{tip} = K_I - L^{1/2}(2/\pi)^{1/2}\sigma_c \int_0^1 \phi(\eta)/(\eta)^{1/2}\,d\eta = 0 \tag{27}$$

which implies that

$$K_I(\pi/2)^{1/2}/(L)^{1/2}\sigma_c = (\lambda/\alpha)^{1/2} = \int_0^1 \phi(\eta)/(\eta)^{1/2}\,d\eta. \tag{28}$$

Substitution of eqn (28) into eqn (22) yields

$$1 = \phi(\xi) + \alpha \int_0^1 \phi(\eta)K(\xi,\eta)\,d\eta \tag{29}$$

where

$$K(\xi,\eta) = 2(\xi/\eta)^{1/2} - \ln|(\xi^{1/2}+\eta^{1/2})/(\xi^{1/2}-\eta^{1/2})|. \tag{30}$$

Note that, the condition that $\sigma = \sigma_c$ at the tip of the bridging zone, i.e.

$$\phi(0) = 1 \tag{31}$$

is automatically satisfied by eqn (29).

Numerical procedure to solve eqn (29) is as follows: we increase α from zero to some final value α_c. For each α, a solution $\phi(\xi,\alpha)$ is obtained. α_c is determined by the fracture condition

$$\phi(\xi = 1, \alpha_c) = 0. \tag{32}$$

Physically, the condition $\sigma = 0$ or $\phi = 0$ at the crack tip must correspond to $\lambda = 1$. Indeed, crack growth is unstable for $\lambda > 1$ since the energy flow to the crack tip exceeds the maximum energy that can be dissipated by the material in the bridging zone.

Numerical solution of the integral eqn (29) is obtained by discretizing (29) into

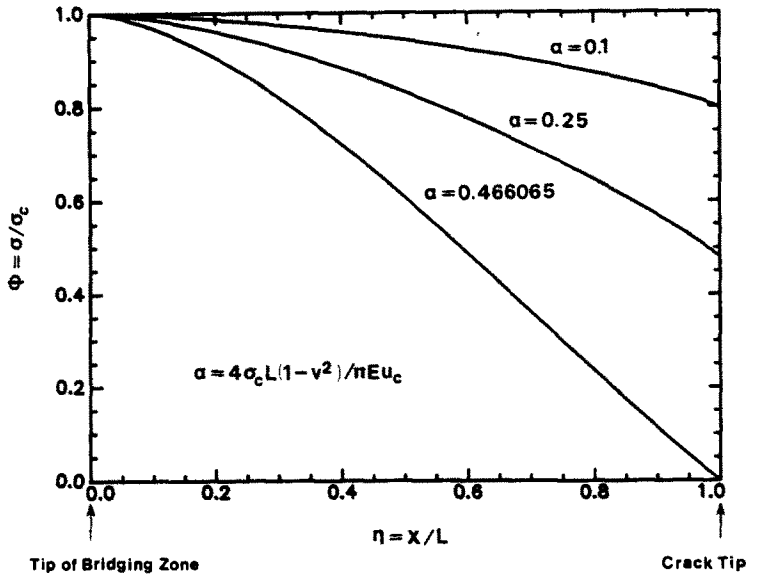

Fig. 7. Plot of normalized stresses vs nondimensional distance from crack tip.

$$f_i = \phi_i + \alpha \sum_{j=1}^{N} \phi_j \int_{\eta_{j-1}}^{\eta_j} K(\xi_i, \eta)\, d\eta, \quad i = 1, 2, \ldots, N. \tag{33}$$

where $f_i = 1$, $\phi_i = \phi(\xi_i)$ and $\eta_0 = 0$. The system of linear algebraic eqns (33) is solved and α_c is found to be

$$\alpha_c = 0.466065. \tag{34}$$

The normalized stresses $\phi(\xi)$ are plotted in Fig. 7 for $\alpha = 0.1, 0.25$, and $\alpha = \alpha_c$ respectively. For $\alpha < \alpha_c$, the condition $0 < \phi(\xi, \alpha) < 1$ is always satisfied.

There is a relationship between the value of the stress at the crack tip and the ratio of the energy release rate λ. This relationship can be obtained by applying the path-independent J-integral

$$J = K_I(1-\nu^2)/E = \int_0^u \sigma(u')\, du' \tag{35}$$

in the bridging zone under small-scale yielding condition (Rice, 1968). For the linear σ–u relation (16), eqn (35) leads to

$$\lambda = 1 - \phi^2(1). \tag{36}$$

A plot of λ vs α is shown in Fig. 8 which indicates that λ is a single-valued increasing function of α. The maximum $L = L_{\max}$ above which instability will occur is determined by the length scale Eu_c/σ_c.

4. DISCUSSION

Our simple analysis indicated that the interaction between debonding and plastic stretching is an important mechanism for fracture toughness enhancement. In our analysis, we have assumed implicitly that there is enough debonding so that the neck geometry shown in Fig. 2b can be realized. In fact, the minimum debonding length needed to achieve the given neck geometry, l_s, is given by

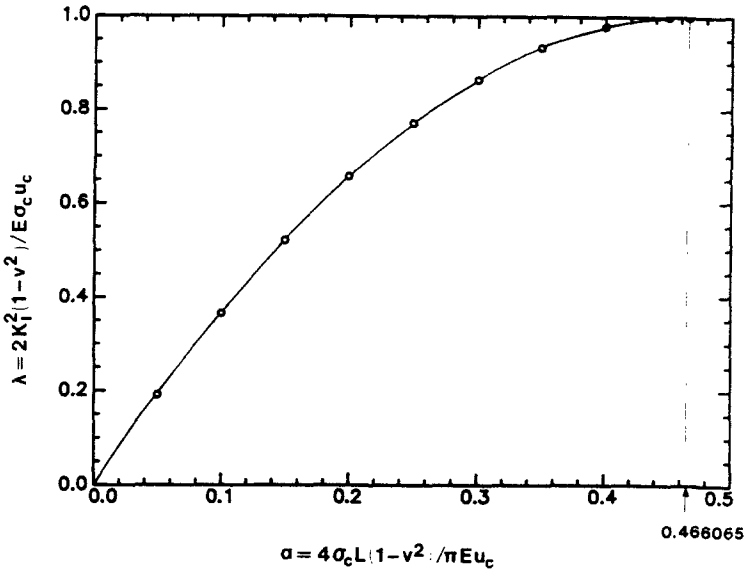

Fig. 8. Plot of $G/\Delta G_p$ vs normalized bridging zone length.

$$l_s/a_0 = R/a_0 - (R/a_0)^2(\pi - 4R/3a_0)/2. \tag{37}$$

Comparison of eqns (1) and (37) shows that for $l_s/a_0 > 0.2$, the neck geometry proposed by Fig. 2b can always be achieved. Furthermore, since the Bridgeman solution depends only on the crack tip curvature (the curvature of the neck ahead of the crack tip), one would expect that the amount of plastic stretching to be an increasing function of the debonded length, as long as the remaining intact interfaces can transmit sufficient forces for continuing deformation. This means that one can expect an optimal debonding length which gives rise to maximum plastic stretching.

We have not taken into account the fracture energy needed to debond the interface. If the interface is modeled as a perfectly plastic two-dimensional continuum with constitutive behavior of the form

$$\begin{aligned} \delta_c > \delta > 0, \quad & \sigma_r = \sigma_b \\ \delta > \delta_c, \quad & \sigma_r = 0 \end{aligned} \tag{38}$$

then the energy needed for partial debonding is:

$$\Delta E = 4f\sigma_b\delta_c l_s/a_0 \tag{39}$$

where δ_c is the critical opening displacement of the interface and σ_b is the interface strength. The increase in fracture toughness due to partial debonding is

$$\Delta G_d = 4f\sigma_b\delta_c/a_0. \tag{40}$$

The total increase in fracture toughness is the sum of the energy dissipated by plastic stretching and debonding, i.e.

$$\Delta G = \Delta G_p + \Delta G_d. \tag{41}$$

For interface models whose restraining stress is an arbitrary function of the opening displacement, $\sigma_b\delta_c$ in eqn (40) should be replaced by

$$\int_0^{\delta_c} \sigma_r(\delta)\,\mathrm{d}\delta. \tag{42}$$

Note that the increase in fracture toughness due to plastic stretching in this model is proportional to the particle size a_0, whereas the fracture toughness increase due to debonding is inversely proportional to a_0 for a given area concentration f. The inverse dependence of ΔG_d on a_0 is a consequence of the fact that for a given concentration of particles, the surface area increases like $1/a_0$.

Our analysis of the effect of debonding on fracture toughness enhancement is based on the assumption that the process of debonding is decoupled from the process of plastic stretching of the particles. This is because the debonded length in our calculation is fixed and remains constant during the stretching process. A more realistic model should take into account the debonding process during particle deformation. Further investigation should study the interaction of debonding and plastic deformation in detail so that a more accurate fracture toughness can be obtained. It is also likely that part of the interface may slip which would lead to further increases in fracture toughness.

The use of the σ–u relation (16) allows us to deduce the bridging zone size as a function of the applied load and material parameters. In our analysis we have assumed that the fracture toughness of the matrix is much smaller than the enhanced toughness provided by the plastic stretching process. This is because the total stress intensity factor is zero in our analysis. This differs from the previous analysis (Budiansky *et al.*, 1988) as the stresses are bounded everywhere.

Acknowledgements—Partial support by the U.S. Army Research Office through the Mathematical Sciences Institute of Cornell University is gratefully acknowledged. C. Y. Hui also acknowledges the partial support of U.S. Army under contract number DAA L03-88-K-0157.

REFERENCES

Budiansky, B., Hutchinson, J. W. and Lambropoulos, J. C. (1983). Continuum theory of dilatant transformation toughening in ceramics. *Int. J. Solids Structures* **19**, 337.

Budiansky, B., Hutchinson, J. W. and Evans, A. G. (1986). Matrix fracture in fiber-reinforced ceramics. *J. Mech. Phys. Solids* **34**, 167.

Budiansky, B., Amazigo, J. C. and Evans, A. G. (1988). Small-scale bridging and the fracture toughness of particulate-reinforced ceramics. *J. Mech. Phys. Solids* **36**, 167.

Evans, A. G. and McMeeking, R. M. (1986). On the toughening of ceramics by strong reinforcements. *Acta metall.* **34**, 2435.

Hutchinson, J. W. (1987). Crack tip shielding by micro-cracking in brittle solids. *Acta metall.* **35**, 1605.

Kristic, V. D., Nicholson, P. S. and Hoagland, R. G. (1981). Toughening of glasses by metallic particles. *J. Am. Ceram. Soc.* **64**, 499.

Kristic, V. D. (1983). On the fracture of brittle–matrix/ductile–particle composites. *Philos. Mag.* **A48**, 695.

McMeeking, R. M. and Evans, A. G. (1982). Mechanics of transformation–toughening in brittle materials. *J. Am. Ceram. Soc.* **65**, 242.

Rice, J. R. (1968). Mathematical analysis in the mechanics of fracture. In *Fracture* (Edited by H. Liebowitz). Academic Press, New York.

Sigl, L. S., Mataga, P. A., Dalgleish, B. J., McMeeking, R. M. and Evans, A. G. (1988). On the toughness of brittle materials reinforced with a ductile phase. *Acta metall.* **36**, 945.

Tada, H., Paris, P. C. and Irwin, G. R. (1973). *The Stress Analysis of Cracks Handbook*. Del Research, Hellertown.

Tirosh, J. and Tetelman, A. S. (1976). Fracture conditions of a crack approaching a disturbance. *Int. J. Fracture* **12**, 187.

APPENDIX

For the model geometry given in Fig. 2b, conservation of volume implies

$$V_1 = V_2, \tag{A1}$$

i.e.

$$V_1 + V_0 = V_2 + V_0. \tag{A2}$$

It is elementary to show that

$$V_2 + V_0 = \pi u a_0^2 \tag{A3}$$

and

$$\begin{aligned} V_1 + V_0 &= 2\pi(a_0 - 4R/3\pi)\pi R^2/2 \\ &= \pi^2 R^2(a_0 - 4R/3\pi). \end{aligned} \tag{A4}$$

Therefore

$$\pi u a_0^2 = \pi^2 R^2(a_0 - 4R/3\pi) \tag{A5}$$

i.e.

$$u/a_0 = (R/a_0)^2(\pi - 4R/3a_0). \tag{A6}$$

When the particle fails (i.e. $R = a_0$)

$$u^* = a_0(\pi - 4/3) = 1.80826a_0. \tag{A7}$$